

Structure of spin-dependent scattering amplitude and spin effects at small angles at RHIC energies

N. A. Khuri

Department of Physics and Astronomy, University of Iowa, Iowa City, IA 52242, U.S.A.

S. V. Goloskokov, O. V. Selyugin

BLTP, Joint Institute for Nuclear Research, 141980 Dubna, Moscow Region, Russia

(April 16, 2024)

Abstract

Spin-dependent pomeron effects are analyzed for elastic pp scattering and calculations for spin-dependent differential cross sections, analyzing power and double-spin correlation parameters are carried out for the energy range of the Relativistic Heavy Ion Collider (RHIC) at BNL. In this energy range, $50 \sqrt{s} = 500$ GeV, the structure of pomeron-proton coupling can be measured at RHIC with colliding polarized proton beams.

I. INTRODUCTION

The spin structure of the pomeron is still an unresolved question in the diffractive scattering of polarized particles. There have been many observations of spin effects at high energies and at fixed momentum transfers [1,2]; several attempts to extract the spin- ρ amplitude from the experimental data show that the ratio of spin- ρ to spin-non- ρ amplitudes can be non-negligible and may be independent of energy [3,4]. In all of these cases, the pomeron exchange is expected to contribute the observed spin effects at some level. The large rapidity events that are observed at CERN [5] and DESY [6], and all diffractive and elastic high energy reactions are predominated by pomeron exchange, thus making the pomeron a popular field of study. Extensive polarized physics programs are proposed at HERA, RHIC and LHC (see e.g. [7-9]) in order to shed light on these and other spin effects in hadron reactions.

It is generally believed, based on calculations of the simplest QCD diagrams, that the spin effects diminish as inverse power of center-of-mass energy, and that the pomeron exchange does not lead to appreciable spin effects in the diffraction region at super-high energies. Complete calculations of the full set of helicity scattering amplitudes in diffraction region cannot be carried out presently since they require extensive treatment of non-perturbative contributions from many diagrams. Semi-phenomenological models, however, have been developed with parameters which are expected to be fixed with the aid of data from experiments [10,11].

Vacuum t -channel amplitude is usually associated with two-gluon exchange in QCD [12]. The properties of the spinless pomeron were analyzed on the basis of a QCD model, by taking into account the non-perturbative properties of the theory [13,14]. We refer to this as the standard-pomeron model in this paper.

Some models predict non-zero spin effects as $s \rightarrow \infty$ and $t, \bar{t} \rightarrow 0$ limit. In these studies, the spin- ρ amplitudes which lead to weakly altered spin effects with increasing energy are connected with the structure of hadrons and their interactions at large distances [10,11]. In

reference [10], the spin-dependence of the pomeron term is constructed to model rotation of matter inside the proton. This approach is based on Chou and Yang's concept of hadronic current density [15]. The model developed in reference [11] considers the contribution of a sea quark-antiquark pair to hadron interactions at large distances.

This picture can be related with the spin effects determined by higher-order s contributions in the framework of PQCD. Really, it has been shown in the framework of QCD analysis at fixed momentum transfer that these corrections to the simple two-gluon exchange [16] may lead to the spin- $\frac{1}{2}$ amplitude growing as s in the limit of $s \rightarrow \infty$. The similar effects can be determined by the quark loops contributions [17]

The high energy two-particle amplitude determined by pomeron exchange can be written in the form :

$$T(s;t) = i s P(s;t) V_{h_1 h_1 P} V^{h_2 h_2 P} : \quad (1)$$

Here P is a function caused by the pomeron, with a weak energy dependence $(\ln s)^{\alpha}$; and V^{hhP} are the pomeron-hadron vertices. The perturbative calculation of the pomeron coupling structure is rather difficult and the non-perturbative contributions are important for momentum transfers of a few $(\text{GeV} = c)^2$.

The calculation of Eq.(1) in the non-perturbative two-gluon exchange model [13] and in the BFKL model [18] shows that the pomeron couplings have the following simple form :

$$V_{hhP} = \gamma_{hhP} : \quad (2)$$

In this case, the pomeron contribution leads to a weak energy dependence of the differential cross section with parallel and antiparallel spins, and their difference drops as inverse power of s , leading us to conclude that the spin effects are suppressed as a power of s .

This situation changes dramatically when large-distance loop contributions are considered which lead to a more complicated spin structure of the pomeron coupling. As mentioned above, these effects can be determined by the hadron wave function for the pomeron-hadron couplings, or by the gluon-loop corrections for the quark-pomeron coupling [19]. As a result,

spin asymmetries appear that have weak energy dependence as $s \rightarrow 1$. Additional spin- ρ contributions to the quark-pomeron vertex may also have their origins in instantons, e.g. [20,21].

In the framework of the perturbative QCD, the analyzing power of hadron-hadron scattering was shown to be of the order:

$$A_N / m_s = \frac{q}{p_t^2}$$

where m_s is about a hadron mass [22]. Hence, one would expect a large analyzing power for moderate p_t^2 where the spin- ρ amplitudes are expected to be important for the diffractive processes.

In this paper, we examine the spin-dependent contribution of pomeron to the differential cross sections with parallel and antiparallel spins, their possible magnitudes and energy dependence. We also estimate the possible experimental precisions for these observables in the RHIC energy domain.

II. THE MODEL AMPLITUDES

We use the standard helicity representation for the hadron-hadron scattering amplitudes: $f_1 = \langle ++ | M | ++ \rangle$ and $f_3 = \langle +- | M | +- \rangle$, helicity non- ρ amplitudes; $f_2 = \langle ++ | M | j- \rangle$ and $f_4 = \langle +- | M | j- \rangle$, double- ρ amplitudes; and $f_5 = \langle ++ | M | j+ \rangle$, single- ρ amplitude. We assume, as usual, that at high energies the double- ρ amplitudes are small with respect to the spin-non- ρ one, $f_2(s;t) = f_4(s;t) = f_1(s;t)$ and that spin-non- ρ amplitudes are approximately equal, $f_+(s;t) = f_1(s;t) = f_3(s;t)$. Consequently, the observables are determined by two amplitudes: $f_+(s;t)$ and $f_-(s;t) = f_5(s;t)$. These customary assumptions are also made for the models developed in [10,11].

We use the below normalization for the differential cross section:

$$\sigma_0 = \frac{d}{dt} = \frac{4}{s(s-4m^2)} (f_+^2 + 2f_-^2);$$

and the analyzing power and the double spin correlation parameters are:

$$A_N = \frac{8}{s(s-4m^2)} \text{Im} [f f_+];$$

$$A_{NN} = \frac{4}{s(s-4m^2)} 2\mathfrak{f} \mathfrak{f}^{\dagger}:$$

The measured spin-dependent differential cross sections can be written in the form :

$$N(\uparrow\uparrow)=L \quad (\uparrow\uparrow) = (\sigma_0=4) [1 + A_N (P_1 + P_2) \cos \varphi + A_{NN} P_1 P_2 \cos^2 \varphi]; \quad (3)$$

$$N(\uparrow\downarrow)=L \quad (\uparrow\downarrow) = (\sigma_0=4) [1 - A_N (P_1 + P_2) \cos \varphi + A_{NN} P_1 P_2 \cos^2 \varphi];$$

$$N(\downarrow\uparrow)=L \quad (\downarrow\uparrow) = (\sigma_0=4) [1 + A_N (P_1 + P_2) \cos \varphi - A_{NN} P_1 P_2 \cos^2 \varphi];$$

$$N(\downarrow\downarrow)=L \quad (\downarrow\downarrow) = (\sigma_0=4) [1 - A_N (P_1 + P_2) \cos \varphi - A_{NN} P_1 P_2 \cos^2 \varphi];$$

$$\sigma_0 = [N(\uparrow\uparrow) + N(\uparrow\downarrow) + N(\downarrow\uparrow) + N(\downarrow\downarrow)]/L:$$

L is the luminosity and σ_0 is the normalized differential cross section. P_1 and P_2 refer to the degree of beam polarizations for the first and second beams, respectively, and φ is the azimuthal scattering angle. The arrows indicate the transverse spin orientations of the interacting protons.

If we adapt the following notation:

$$(\uparrow) = [N(\uparrow\uparrow) + N(\uparrow\downarrow)]/L; \quad (\downarrow) = [N(\downarrow\downarrow) + N(\downarrow\uparrow)]/L;$$

$$(\uparrow\uparrow) = [N(\uparrow\uparrow) + N(\downarrow\downarrow)]/L; \quad (\uparrow\downarrow) = [N(\uparrow\downarrow) + N(\downarrow\uparrow)]/L;$$

then, the analyzing power, A_N , and the double-spin correlation parameter, A_{NN} , can be extracted from the experimental measurements;

$$A_N = \frac{(\uparrow) - (\downarrow)}{(\uparrow) + (\downarrow)} = \frac{s}{\sigma_0} = \frac{2\text{Im}(f f_+)}{\mathfrak{f}_+ \mathfrak{f}^{\dagger} + 2\mathfrak{f} \mathfrak{f}^{\dagger}}; \quad (4)$$

$$A_{NN} = \frac{(\uparrow\uparrow) - (\uparrow\downarrow)}{(\uparrow\uparrow) + (\uparrow\downarrow)} = \frac{d}{\sigma_0} = \frac{2\mathfrak{f} \mathfrak{f}^{\dagger}}{\mathfrak{f}_+ \mathfrak{f}^{\dagger} + 2\mathfrak{f} \mathfrak{f}^{\dagger}}; \quad (5)$$

Hereafter, s and d refer to the single- and double-spin cross section differences. We follow the model developed in [11] closely and extend it further for the calculation of spin-dependent differential cross sections. Pomeron-proton coupling V_{ppP} is primarily connected with the proton structure at large distances and the pomeron-proton coupling looks like:

$$V_{ppP}(p;t) = m_p A(t) + B(t); \quad (6)$$

where m is the proton's mass, p is the hadron momentum and t is the four-momentum transfer square. $B(t)$ is a standard pomeron coupling that determines the spin-non flip amplitude. The term $m_p A(t)$ is due to meson-cloud effects. This coupling leads to spin-flip at the pomeron vertex which does not vanish in the $s \rightarrow \infty$ limit. Using Eq.(6), we can calculate the spin-non flip and spin-flip amplitudes from the pomeron-proton vertex:

$$\frac{f_+(s;t)}{f(s;t)} = \frac{m_p A(t)}{B(t)} \quad (7)$$

Hence, V_{ppP} determine A_N and A_{NN} parameters. Both of the above amplitudes have the same energy dependence and the ratio of spin-flip to spin-non flip amplitudes in this picture gives:

$$\frac{m_p f_+(s;t)}{f_+ f(s;t)} = \frac{m_p^2 A(t)}{B(t)}, \quad 0.05 \text{ to } 0.07 \text{ for } t \approx -0.5 \text{ (GeV}^2\text{)} \quad (8)$$

which is consistent with other estimates [3].

The amplitudes A and B have a phase shift caused by the soft pomeron rescattering. As a result, the analyzing power determined by the pomeron exchange

$$A_N \frac{d}{dt} = 2m_p \frac{f_+}{f} \text{Im}(AB) \quad (9)$$

and appears to have a weak energy dependence.

The model also takes into account the contributions of the Regge terms to both f_+ and f amplitudes. So, the scattering amplitudes are

$$f(s;t) = i s [f^{as} + \frac{(c_1 - i q)}{p - s} f_+^{reg} + \frac{c_3 (1 + i)}{p - s} f^{reg}] = i s [f^p + f^r]; \quad (10)$$

where f^{as} ; f^{reg} are functions which weakly depend on energy and c_i are parameters. The asymptotic terms f^{as} and f^{reg} were calculated in the framework of the model [11]. The Born amplitudes in the form of Eq.(7) are modified by pomeron rescattering. The Regge

contributions, Eq.(10), were represented in the simplest exponential form. These, and some of the asymptotic function parameters, were obtained from the fit to the experimental data (for details see [11]). The model quantitatively describes all the known experimental data of the proton-proton and proton-antiproton scattering, from $\sqrt{s} = 10 \text{ GeV}$ up to $\sqrt{s} = 1.8 \text{ TeV}$ [11,24]. We thus expect the predictions for differential cross sections at RHIC energies to be reliable. We neglect a possible odderon contribution in these calculations.

III. SPIN CORRELATION EFFECTS

The meson-cloud [11] and the rotating matter current [10] models quantitatively describe the experimental data on elastic pp scattering at fixed momentum transfers and can predict physical observables (cross sections and asymmetries) at high energies. The predictions, however, differ in size and sign for asymmetries.

We calculate the spin-dependent cross sections using the above described amplitudes in Eq.(10), and we use the parameters of the RHIC beams [9] for the estimation of statistical errors. We assume at $\sqrt{s} = 200 \text{ GeV}$, the luminosity is $L = 3 \cdot 10^{31} \text{ cm}^{-2} \text{ sec}^{-1}$ and the average beam polarization per beam is 70%. The typical geometrical acceptance of the detector is taken to be 20% and the running time is about a month. The momentum transfer binning, we take $t = 0.05 \text{ (GeV=c)}^2$ at $|\mathbf{t}| = 1.3 \text{ (GeV=c)}^2$ and $t = 0.1 \text{ (GeV=c)}^2$ at $|\mathbf{t}| = 1.3 \text{ (GeV=c)}^2$.

The energy dependence of the real part of the non ip amplitudes around diffraction minimum ($\text{Im } f_{\pm}(s;t) = 0$), is model dependent and may lead to different polarization predictions in this momentum transfer range.

The local dispersion relations have been used in [11] to determine the real part of $T(s;t)$. The model amplitude obeys the s u crossing symmetry which permits us to describe quantitatively all the specific effects in the elastic proton-proton and proton-antiproton diffraction scattering in the wide energy region ($9.8 \text{ GeV} \leq \sqrt{s} \leq 1800 \text{ GeV}$). For example, model describe the difference of the differential cross sections for proton-proton and

proton-antiproton scattering in domain of the diffraction minimum, the known polarization phenomena at $\sqrt{s} = 9.8 \text{ GeV}$ and $\sqrt{s} = 52.8 \text{ GeV}$ and the experimental data of proton-antiproton scattering at $\sqrt{s} = 540$ and 630 GeV . All these quantities are sensitive to the real part of the scattering amplitude. So, we can believe that $\text{Re}[T(s;t)]$ determined correctly and practically model-independent.

The differential cross section calculations are shown in Fig. 1 a,b. The estimated errors are statistical and are less than 1%. At $\sqrt{s} = 50 \text{ GeV}$, the model described here quantitatively reproduces the ISR data [23]. The diffraction minimum defined by the zero of the imaginary part of the spin-non ip amplitude is filled by the contributions of the real-part of spin-non ip and spin-ip amplitudes. At $\sqrt{s} = 120 \text{ GeV}$, the dip becomes a shoulder and increases by an order of magnitude when the energy goes from $\sqrt{s} = 120 \text{ GeV}$ to 500 GeV . The model gives the same asymptotical predictions for the proton-proton and proton-antiproton differential cross sections. Hence the cross section prediction at $\sqrt{s} = 500 \text{ GeV}$ approximately corresponds to the SppS data at $\sqrt{s} = 540 \text{ GeV}$.

Fig 2 a,b show calculations for d as determined in Eq.(5). It can be seen that the shape of d is similar to the spin-averaged differential cross sections. It has a sharp dip and the magnitude of d at the dip grows by an order of magnitude in the energy interval $120 \leq \sqrt{s} \leq 500 \text{ GeV}$. Although the dip positions for differential cross sections and that of d seem to coincide at $\sqrt{s} = 50 \text{ GeV}$ but at higher energies they move apart from each other since the dip of d moves more slowly. The position of the d minimum strongly depends on the model parameters. However, in the ranges of $t, t' = 0.7$ to $1.0 (\text{GeV} = c)^2$ and $t, t' = 1.8 (\text{GeV} = c)^2$, the results weakly depend on these parameters. In the regions far from the dips, both cross sections change slowly, especially at $t, t' = 2 (\text{GeV} = c)^2$.

The energy dependence of $f_+(s;t)$ and $f_-(s;t)$ amplitudes are determined in Eq.(7) for the V_{ppP} vertex. Hence, we have the same energy dependence for d and $\langle \sigma \rangle$ for the spin-pomeron models, and the ratio of these quantities will be almost energy independent, except around the diffraction minimum.

The calculated ratio of the spin-parallel and antiparallel cross sections, $R(s;t) =$

$\rho'' = \rho''^{\#}$, shows only a logarithmic dependence on energy in its first maximum and is almost energy independent at $\sqrt{s} = 0.7$ (GeV/c)², see (Fig. 3 a,b). It is clear from these results that the spin effects can be sufficiently large at all RHIC energies.

Relative errors in $R(s;t)$ are shown in Table I at two selected momentum transfers and at t_m where the first maximum of $R(t)$ is observed. It is worthwhile to note that the errors with the growth of energy decrease due to increase in the differential cross sections. Also note that in all standard pomeron models this ratio is predicted to be

$$R(s;t) = \rho'' = \rho''^{\#} \rightarrow 1 \text{ as } s \rightarrow \infty :$$

However, the experiment data show a large deviation from unity [1]. It is also interesting that at low-energies ($\sqrt{s} = 11.7$ and 18 GeV/c) [25,26], $R(s;t)$ does not change much with energy at $\sqrt{s} \approx 2$ (GeV/c)² and is similar to our predictions of $R(s;t)$ at the first maximum.

Our calculation for A_N is shown in Fig. 4 a,b. The magnitude and the energy dependence of this parameter depend on the energy behavior of the zeros of the imaginary-part of spin- $\frac{1}{2}$ amplitude and the real-part of spin-non $\frac{1}{2}$ amplitude.

The maximum negative values of A_N coincide closely with the diffraction minimum (see Figs. 1 and 4). We find that the contribution of the spin- $\frac{1}{2}$ to the differential cross sections is much less than the contribution of the spin-non $\frac{1}{2}$ amplitude in the examined region of momentum transfers from these figures. A_N is determined in the domain of the diffraction dip by the ratio

$$A_N = \frac{\text{Im } f = \text{Re } f_+}{\text{Re } f_-} : \quad (11)$$

The size of the analyzing power changes from 45% to 50% at $\sqrt{s} = 50$ GeV up to 25% at $\sqrt{s} = 500$ GeV. These numbers give the magnitude of the ratio Eq.(11) that does not strongly depend on the phase between the spin- $\frac{1}{2}$ and spin-non $\frac{1}{2}$ amplitudes. This picture implies that the diffraction minimum is filled mostly by the real-part of the spin-non $\frac{1}{2}$ amplitude and that the imaginary-part of the spin- $\frac{1}{2}$ amplitude increases in this domain as well.

We observe that the dips are different in speed of displacements with energy from Figs. 1 and 2. In Fig. 4, one sees that at larger momentum transfers, $t \sim 2$ to 3 (GeV 2), the analyzing power depends on energy very weakly.

The expected errors for the analyzing power are small in nearly all momentum transfer ranges examined. They are summarized in Table II.

As pointed out before, the model [10] predicts a similar absolute value but opposite sign for A_N near the diffraction minimum. The future P P 2P P experiment at RHIC [9] should be able to provide data and help resolve these issues on the mechanism of spin-ect generation at the pomeron-proton vertex.

IV . C O N C L U S I O N

In the framework of the standard-pomeron model, the spin- ip amplitude is defined only by the secondary Regge poles and the ratio

$$[\rho'') \quad \rho'')] = \rho'') / 1 = s$$

that rapidly decreases with growing s due to the standard energy dependence of the spin- ip amplitude. If we drop the asymptotic term in the spin- ip amplitude from Eq.(10) and keep only the second Regge terms that fall as $1 = \frac{P}{s}$, we obtain the pre-asymptotic Regge contributions to the analyzing power and the difference of the polarized cross sections (the results are shown in Fig. 5 and 6).

The spin- ip amplitude of the second Regge contributions has a large relative phase compared to the spin-non ip amplitude of the pomeron. Under this condition, too, the analyzing power can be large. As one observes from Fig. 5, the spin- ip amplitude defined by the Regge contributions can describe the experimental data at $\frac{P}{s} = 23.4$ GeV and give large effects at $\frac{P}{s} = 50$ GeV. At higher energies, however, the effect quickly falls and becomes insignificant. Note that at $\frac{P}{s} = 50$ GeV, A_N can be positive and that its magnitude greatly depends on the size of the asymptotic term which gives a negative contribution to the analyzing power.

If the spin- ρ amplitude is determined by the standard pomeron model, its contribution will be clearly seen in experiments (see Figs 5, 6) if performed. In this case, the minimum in σ^d is at small momentum transfers $|t| \approx 0.7 \text{ (GeV}^2\text{=c}^2\text{)}$, and is quickly shifted with growing energy. In the ordinary dip region, there is a maximum in the difference of the cross sections which falls as the inverse power of energy. Moreover, at $|t| \approx 2 \text{ (GeV}^2\text{=c}^2\text{)}$, in the spin-pomeron model, σ_0 and σ^d do not appreciably change with energy at fixed t (Figs. 1,2). The difference spin-dependent cross sections fall with energy as quickly as the increasing momentum transfers (Fig. 6).

The energy dependence of cross sections σ'' and $\sigma^\#$ can be studied experimentally at RHIC. Note that significant spin effects can have small relative errors at momentum transfers $|t| \approx 2$ to $3 \text{ (GeV}^2\text{=c}^2\text{)}$ and direct information about the nature of the spin- ρ effects in the pomeron-proton coupling can be obtained. The future P P 2P P experiment at RHIC should be able to measure the spin-dependent cross section with parallel σ'' and antiparallel $\sigma^\#$ beam polarizations in proton-proton scattering and the energy dependence of the spin- ρ and spin-non ρ amplitudes can be studied in the energy range of RHIC, $50 \leq \sqrt{s} \leq 500 \text{ GeV}$.

The spin-structure of the pomeron couplings are determined by the large-distance gluon-loop correction or by the effects of hadron wave function. Tests of the spin structure of QCD at large distances can be carried out in diffractive reactions in future polarized experiments at HERA, RHIC and LHC.

ACKNOWLEDGMENTS

The authors are grateful to A.V.Efremov, W.D.Nowak, S.B.Nurushev and A.Penzo for fruitful discussions.

REFERENCES

- [1] K .Abe et al, Phys.Rev.D 16, 549 (1977).
- [2] S.B .Nurushev, Proc.of III W orkshop on High Energy Spin Physics, Protvino, (1989) p.5.
- [3] N .Akchurin, N .H .Buttmonre and A .Penzo, Phys.Rev.D 51, 3944 (1995).
- [4] O .V .Selyugin, Phys.Lett.B 333, 245 (1993).
- [5] A .Brandt et al, Phys.Lett.B 297, 417 (1992).
- [6] T .Ahmed et al, Phys.Lett.B 348, 681 (1995).
- [7] G .Bunce et al, Physics W orld 3, 1 (1992).
- [8] W .D .Nowak, in High Energy Spin Physics, Woodbury, N.Y ., 1995, edited by K .J. Heller and S.L.Smith, AIP Conf.Proc.No.343 (AIP, New York, 1995), p.412.
- [9] W .Guryn et al, Total and Differential Cross Sections and Polarization Effects in pp Elastic Scattering at RHIC (unpublished).
- [10] C .Bourrely, J.Soffer and T .T .Wu, Phys.Rev.D 19, 3249 (1979).
- [11] S.V .Goltskov, S.P.Kuleshov and O .V .Selyugin, Z.Phys.C 50, 455 (1991).
- [12] F.E .Low, Phys.Rev.D 12, 163 (1975); S.Nussinov, Phys.Rev.Lett.34, 1286 (1975).
- [13] P.V .Landshof and O .Nachtmann, Z.Phys.C 35, 405 (1987).
- [14] A .Donnachie and P.V .Landshof, Nucl.Phys.B 311, 509 (1989).
- [15] T .Chou and C .N .Yang, Nucl.Phys.B 107, 1 (1976).
- [16] S.V .Goltskov, Yad.Fiz. 49, 1427 (1989).
- [17] S.V .Goltskov, Z.Phys.C 52, 329 (1991); S.V .Goltskov, J.Phys.G :Nucl.Part.Phys.19, 67 (1993).

- [18] E. A. Kuraev, L. N. Lipatov and V. S. Fadin, Sov. Phys. JETP 44, 443 (1976); Y. Y. Balitsky and L. N. Lipatov, Sov. J. Nucl. Phys. 28, 822 (1978).
- [19] S. V. Goloskokov, Phys. Lett. B 315, 459 (1993).
- [20] A. E. Dorokhov, N. I. Kochelev and Yu. A. Zubov, Int. Jour. Mod. Phys. A 8, 603 (1993).
- [21] M. Anselmino and S. Forte, Phys. Rev. Lett. 71, 223 (1993).
- [22] A. V. Efremov and O. V. Teryaev, Phys. Lett. B 150, 383 (1985).
- [23] S. V. Goloskokov, S. P. Kuleshov and O. V. Selyugin, Yad. Fiz., 46 597 (1987).
- [24] S. V. Goloskokov and O. V. Selyugin, Mod. Phys. Lett. A 9 1207 (1994).
- [25] D. C. Rabb et al., Phys. Rev. Lett. 41 1257 (1978).
- [26] D. C. Rabb et al., Phys. Rev. Lett. 60 2351 (1988).

TABLES

TABLE I. The expected relative errors for $R(s;t) = \langle \sigma \rangle = \langle \sigma \rangle^{\#}$ are tabulated below at $\sqrt{s_1} = 0.5 \text{ (GeV=c)}^2$, $\sqrt{s_2} = 2.5 \text{ (GeV=c)}^2$ and at t_m , where $R(s;t)$ is maximum .

$\sqrt{s} \text{ [GeV]}$	$R(t_1)$	$R(t_m)$	$R(t_2)$
50	0.05%	5.5%	4.1%
120	0.07%	2.2%	4.1%
250	0.07%	1.1%	3.7%
500	0.09%	0.6%	3.6%

TABLE II. The expected relative errors for A_N are calculated at $\sqrt{s_1} = 0.5 \text{ (GeV=c)}^2$, $\sqrt{s_2} = 2.5 \text{ (GeV=c)}^2$ and at t_m , where A_N is maximum .

$\sqrt{s} \text{ [GeV]}$	$A_N(t_1)$	$A_N(t_m)$	$A_N(t_2)$
50	3.1%	3.7%	16%
120	2.3%	2.0%	20%
250	3.5%	1.4%	18%
500	12.4%	1.1%	17%

FIGURES

FIG . 1. a) The calculated differential cross sections of the pp elastic scattering at $s^{1=2} = 50 \text{ GeV}$ (solid curve) and at $s^{1=2} = 120 \text{ GeV}$ (dashed curve); b) $s^{1=2} = 250 \text{ GeV}$ (dotted curve) and at $s^{1=2} = 500 \text{ GeV}$ (dashed curve). The energy range between 50 GeV and 500 GeV correspond to the entire RHIC energy for polarized protons.

FIG . 2. a, b) The calculated difference of the double spin differential cross sections at the RHIC energy range. The error bars indicate possible statistical errors for a realistic experiment at RHIC.

FIG . 3. a, b) The calculated ratio of the cross sections with parallel and antiparallel spins at the RHIC energy range. The error bars indicate possible statistical errors for a realistic experiment at RHIC.

FIG . 4. The calculated analyzing power of the pp elastic cross sections for the weak energy dependence obtained in the model for the ratio $\frac{F^+(s;0) - F^{++}(s;0)}{F^+(s;0) + F^{++}(s;0)}$ a) at $s^{1=2} = 50 \text{ GeV}$ (solid curve) and at $s^{1=2} = 120 \text{ GeV}$ (dashed curve); b) $s^{1=2} = 250 \text{ GeV}$ (dotted curve) and at $s^{1=2} = 500 \text{ GeV}$ (dashed curve). The error bars indicate expected statistical errors for a realistic experiment at RHIC.

FIG . 5. The analyzing power for the pp elastic cross sections for the rapid energy dependence of the ratio $\frac{F^+(s;0) - F^{++}(s;0)}{F^+(s;0) + F^{++}(s;0)}$ (the experimental data at $P_L = 300 \text{ GeV}$ are represented by open circles); the results of calculations are shown for $P_L = 300 \text{ GeV}$ (solid curve); at $s^{1=2} = 50 \text{ GeV}$ (long-dashed curve); at $s^{1=2} = 120 \text{ GeV}$ (short-dashed curve); and at $s^{1=2} = 500 \text{ GeV}$ (dotted curve).

FIG . 6. The calculated difference of the double spin differential for the rapid energy dependence of the ratio $\frac{F^+(s;0) - F^{++}(s;0)}{F^+(s;0) + F^{++}(s;0)}$. The center-of-mass energy span corresponds to the RHIC energy and each curve shows the results at four different cms energies as indicated on the figure.

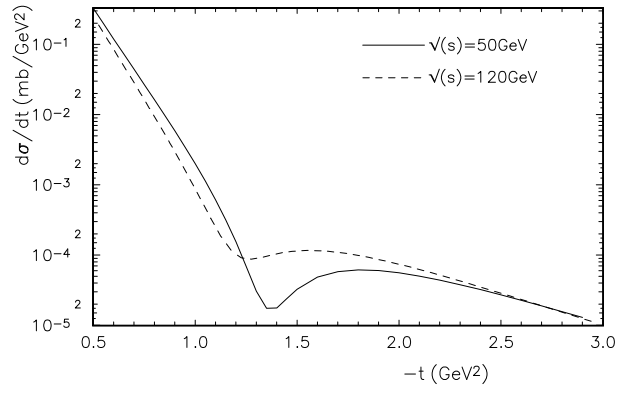


Fig 1 a

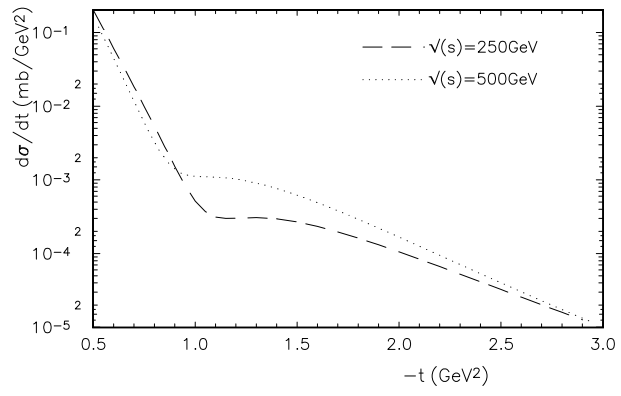


Fig 1 b

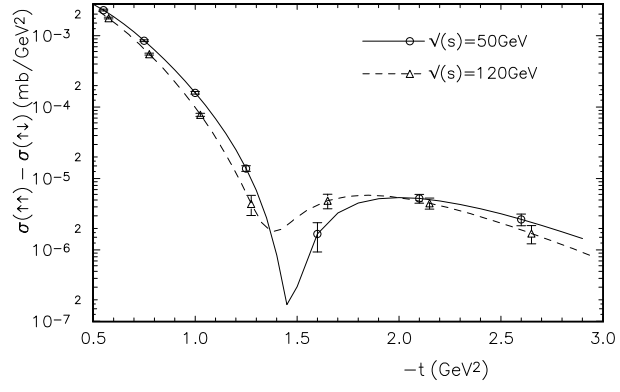


Fig2 a

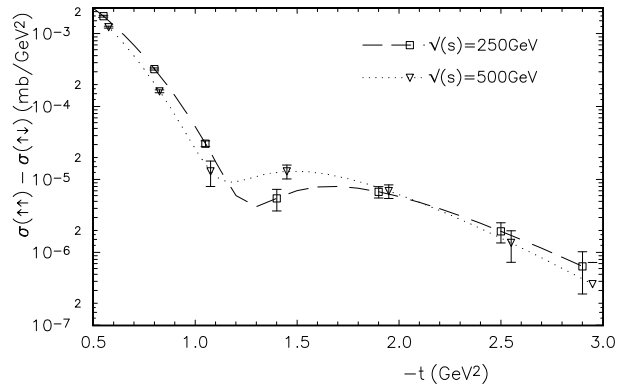


Fig2 b

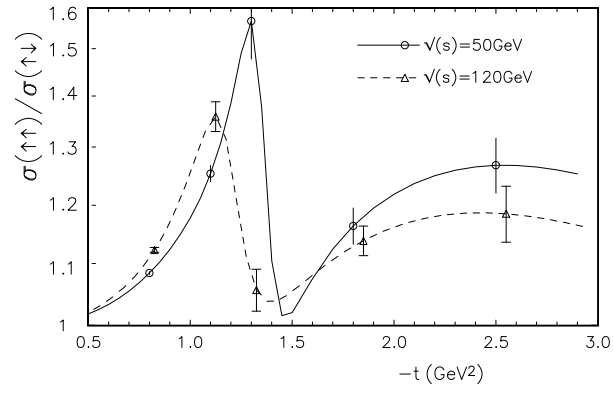


Fig.3 a

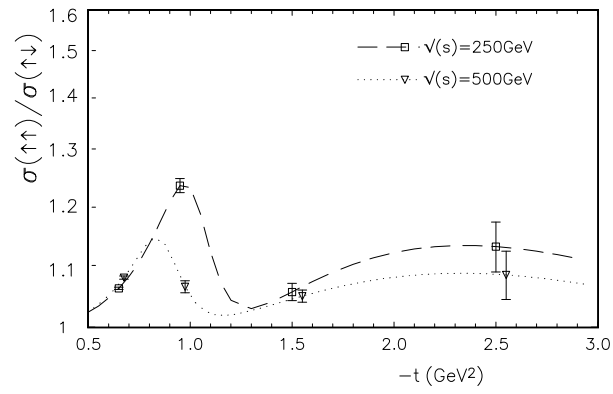


Fig.3 b

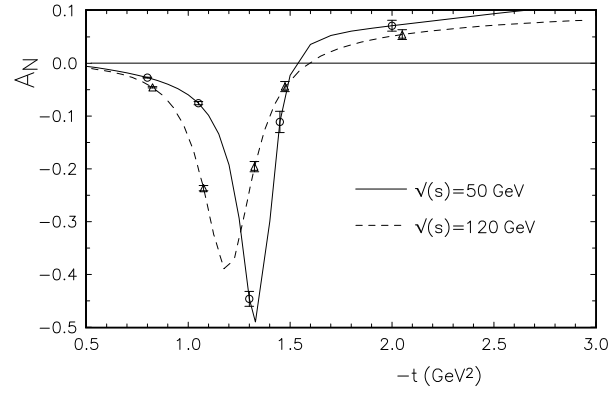


Fig.4 a

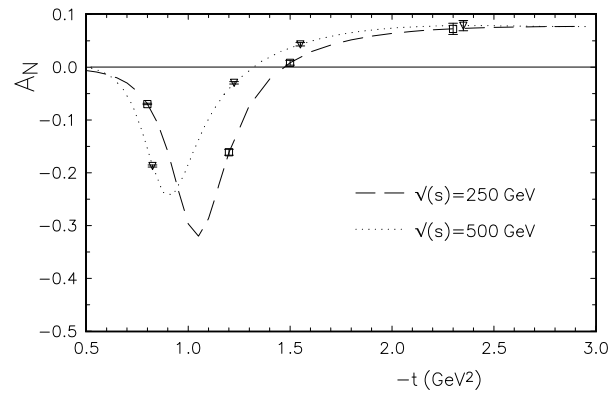


Fig.4 b

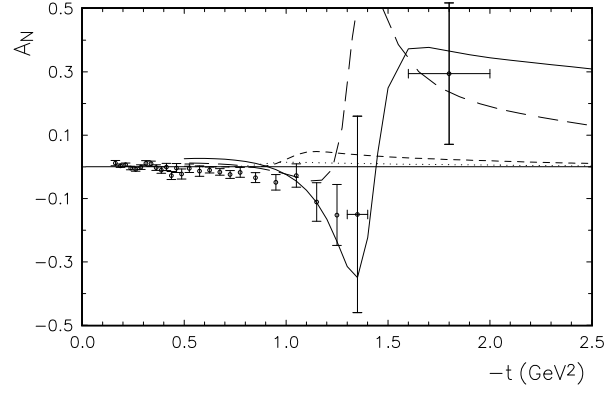


Fig.5

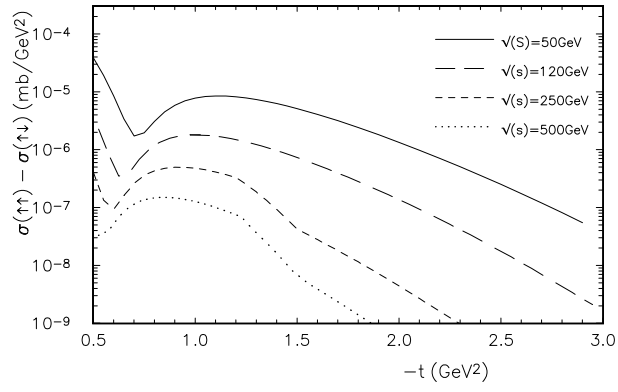


Fig.6